Microelasticity of red blood cells in sickle cell disease

J L Maciaszek[1], B Andemariam[2], and G Lykotrafitis[1]*
[1]Department of Mechanical Engineering, University of Connecticut, Storrs, Connecticut, USA
[2]Department of Medicine, University of Connecticut Health Center, Farmington, Connecticut, USA

Abstract: Translation of cellular mechanics findings is crucial in many diseases, including Alzheimer's disease, Parkinson's disease, type II diabetes, malaria, sickle cell disease, and cancer. Atomic force microscopy (AFM) is appropriate for measuring mechanical properties of living and fixed cells due to its high force sensitivity and its ability to measure local and overall properties of individual cells under physiological conditions. A systemic force–displacement curve analysis is reported on the quantification of material stiffness via AFM using two theoretical models derived from the Hertz model. This analysis was applied to red blood cells from patients with sickle cell disease to determine the Young's modulus of these cells in the oxygenated and deoxygenated state. Sickle cell disease pathophysiology is a consequence of the polymerization of sickle hemoglobin in red blood cells upon partial deoxygenation and the impaired flow of these cells in the microcirculation. A model is presented for a four-sided pyramidal indenter that is subsequently shown to have a better fit to the obtained data than that using a model of a parabolic indenter. It is concluded that deoxygenation and therapeutic treatment have a significant impact on the stiffness. This analysis presents a new approach to addressing medical disorders.

Keywords: atomic force microscopy, cellular mechanics, elasticity, Young's modulus, nanoindentation

1   INTRODUCTION

A detailed knowledge of the mechanical properties of the cell is required if an understanding is to be obtained on how mechanical stresses and deformations regulate cellular functions including fundamental cell processes including mechano-transduction, growth, differentiation, protein and DNA synthesis, motility, and apoptosis [1, 2]. The most common approach reported to study cell mechanics is to determine the stiffness or an apparent elastic modulus of the cell, assuming that it is an elastic body. Atomic force microscopy (AFM) [3] is appropriate for measuring the

mechanical properties of living and fixed cells due to its high force sensitivity and its ability to measure local and overall properties of individual cells under physiological conditions [4–10]. AFM allows simultaneous evaluation of the local mechanical properties and the morphology of the living cells at a high spatial resolution and force sensitivity. The basic technique for quantitative study of the mechanical characteristics of cells and tissues via AFM is force–displacement curve analysis. By recording the force–displacement curves on the sample surface, vertical deflection of the cantilever represents a basis for estimation of a sample's Young's modulus. In the current study, force–displacement curve analysis is used to explore the pathophysiology of sickle cell disease. Understanding the relationship between proteins and cellular material properties will allow for detection of diseases and new approaches to addressing medical disorders [11].

*Corresponding author: Department of Mechanical Engineering, University of Connecticut, 191 Auditorium Road, Unit 3139, Storrs, CT 06269, USA.
e-mail: gelyko@engr.uconn.edu*

2 SICKLE CELL DISEASE

This paper studies the Young's modulus of red blood cells (RBCs, erythrocytes) from patients with sickle cell disease (SCD), a severe disease caused by polymerization of abnormal hemoglobin [12], a globular protein which transports oxygen from the lungs to tissues [13]. Hemoglobin (Hb) is formed by two type α and two type β polypeptide chains. In sickle cell hemoglobin (HbS), the normal sequence of Val-His-Leu-Thr-Pro-Glu-Glu-Lys is changed to Val-His-Leu-Thr-Pro-Val-Glu-Lys, with the amino acid valine substituting for the glutamic acid in the $\beta6$ site. The replacement of two charged groups by two hydrophobic ones leads to polymerization of deoxygenated Hb and to formation of long stiff rod-like fibres [14–16], which force RBCs to assume a wide variety of irregular shapes [17]. The fibres form non-covalent cross-links and create a gel that gives RBCs their irregular shapes and alters their viscoelastic behaviour, increases their rigidity, fragility, and cytoadherence [16, 18–21]. Other factors such as lowered pH, RBC dehydration, and hyperthermia are also known to prompt sickling [22]. Pathology in SCD begins with loss of deformability and increased cell adherence of the sickle cells resulting in serious and often life-threatening complications such as chronic hemolytic anemia and vaso-occlusion [20, 23–25]. People who display a sickle cell trait (SCT) have only one abnormal hemoglobin β gene producing thus both normal hemoglobin (HbA) and sickle hemoglobin HbS with a prevalence of HbA [26, 27].

In the case of SCD, it has been hypothesized that increased association of HbS with the membrane proteins contributes to the change of the mechanical behaviour of sickle erythrocytes [28]. HbS can alter the mechanical properties of RBCs not only by extending the spectrin filaments, and by the interaction between HbS filaments and the lipid bilayer but also by altering the functionality of the membrane proteins [29]. It is known that Hb interacts with the spectrin network via the protein band 3 [30–32] and the introduction of HbS has recently been found to have an effect on the mechanical properties of SCT erythrocytes [33]. In the present study, AFM techniques are used to measure the Young's modulus of RBCs from patients with SCD under both oxygenated and fully deoxygenated conditions.

3 PROBING CELL ELASTICITY USING AFM

In the current work, nanoindentation of RBCs is performed in order to measure the local cell stiffness.

The measurements are performed via AFM by pushing a tip onto the surface of the sample at the position of interest. From the resulting force–displacement curves the local Young's modulus is determined.

3.1 Introduction to contact problems

The general theory of elasticity has been applied to AFM measurements based on the contact theory of Hertz and Sneddon [34–36]. The AFM stiffness measurement is modelled as an indentation of an elastic half-space, $z < 0$, by a frictionless rigid punch [37], as shown in Fig. 1. The profile of the punch is described by the function $f(x, y)$, and $u_z(x, y)$ is the normal deformation of the indented elastic half-space surface. In this case, the half-space represents the indented RBC. The gap $g(x, y)$ between the punch and the half-space is defined as

$$g(x,y) = u_z(x,y,0) - f(x,y) \geq 0 \tag{1}$$

When the shape of the used indenter exhibits a twofold symmetry (e.g. pyramidal or parabolic) then the contact area A preserves the same symmetry as the base of the indenter, with the centre of A being at the coordinate origin ($x = 0$, $y = 0$, $z = 0$). The contact tractions act normal to the surface and are compressive inside A and zero exactly at the contact perimeter, as well as outside A.

The gap is zero within the contact region A and positive in the separation region $\bar{A}$, since interpenetration of material is prohibited. Therefore, the following two conditions can be written

$$u_z(x,y,0) = f(x,y) \ in \ A \tag{2}$$

$$u_z(x,y,0) > f(x,y) \ in \ \bar{A} \tag{3}$$

The definition of the frictionless contact problem is completed by assuming that the tangential traction is zero throughout the surface of the half-space

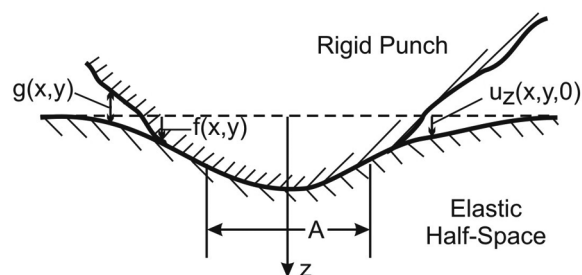$$\sigma_{zx} = \sigma_{zy} = 0 \ all \ x, y, z = 0 \tag{4}$$

Fig. 1 The general indentation problem for a smooth, rigid, frictionless punch

and that the contact pressure $p(x, y) = -\sigma_{zz}(x, y, 0)$ is zero in the separation region $\bar{A}$ and positive in the contact region $\bar{A}$, that is

$$p(x, y) = 0 \text{ in } \bar{A} \tag{5}$$

$$p(x, y) > 0 \text{ in } A \tag{6}$$

If the contact region A is specified, the equality conditions (2), (4), (5) define a well-posed boundary value problem for the half-plane which has a unique solution. Then, the total contact force is obtained by

$$P_z = \iint_A p(x, y) \mathrm{d}x \mathrm{d}y \tag{7}$$

The inequalities (3) and (6) serve to determine the extent of the contact area for the contact problem, but it has been shown [38] that the value of A, which satisfies equations (3) and (6), maximizes the total force P_z given by equation (7).

In the case of a spherical indenter, by solving the boundary contact problem as performed by Hertz [35], the following result is obtained

$$P_z(r_s) = p_0 \sqrt{a^2 - r_s^2} \tag{8}$$

where $s = |r| = \left(r^2 + r_s^2 - 2rr_s \cos\theta + u_z^2\right)^{1/2}$ is the distance between source $(r_s, 0, 0)$ and observation point (r, θ, u_z) is the angular distance, and $p_0 = 2E/\pi R(1 - \nu^2)$, where E is the Young's modulus. The contact radius, a, is given in terms of the applied force, F, and the Poisson's ratio, ν, of the sample

$$a = \left(\frac{4}{3} \times \frac{1 - \nu^2}{E} \times FR\right)^{1/3} \tag{9}$$

Sneddon extended the Hertz model from a spherical indenter to an indenter of arbitrary profile deforming elastic half-space [36, 39]. Solutions of the boundary contact problem for other tip geometries with twofold symmetry generated models for parabolic [40–42] and pyramidal [39, 43–45] indenters. The general solution for force as a function of indentation for a parabolic indenter can be approximated as

$$F_{\text{parabolic}} = \frac{4}{3} \sqrt{RE'} \, u_z^{3/2} \tag{10}$$

where E' is the reduced Young's modulus of the tip–sample system defined as

$$\frac{1}{E'} = \frac{1 - \nu^2}{E} \tag{11}$$

The general solution for force as a function of indentation for a pyramidal indenter [43–45] can be approximated as

$$F_{\text{pyramid}} = \frac{3E \tan\theta}{4(1 - \nu^2)} u_z^2 \tag{12}$$

3.2 Contact problems in AFM

In a force curve on a sample indented via AFM, the indentation, u_z, is equal to

$$u_z = d - \delta \tag{13}$$

where δ is the deflection of the cantilever on the rigid substrate and d is the deflection of the cantilever on the indented half-space. In this particular study, δ is the deflection of the cantilever on the poly-l-lysine coated mica substrate and d is the deflection of the cantilever on the indented erythrocyte surface.

Three important assumptions used in the Hertz–Sneddon model are:

(a) the indenter must have a parabolic shape;
(b) the indented sample is assumed to be extremely thick in comparison to the indentation depth;
(c) there is no adhesive interaction between the sample and the indenter.

The first assumption remains a valid one for the case when a spherical tip radius is much larger than the indentation depth $(u_z < 0.3R)$ [46]. The second assumption states that elastic models based on Hertz–Sneddon contact mechanics are accurate when the indentation depth is small compared to the thickness of the cell. This corresponds with the well-known fact that the effect of the substrate over which the cells are placed is negligible if the indentation depth is less than 10 per cent of the total thickness of the specimen [47]. In cases where the third assumption is not satisfied, the Johnson–Kendall–Roberts (JKR) model should be applied to incorporate the effect of adhesion [48]. The JKR model considers the effect of contact pressure and adhesion within the area of contact. In the current study, no pull-off or rupture forces were observed in the experimental force–distance curves as shown in Fig. 2. This can be attributed to the fact that the AFM indenter used in these experiments was not functionalized. Therefore, the Hertz–Sneddon model appropriately describes the measurements in the present study.
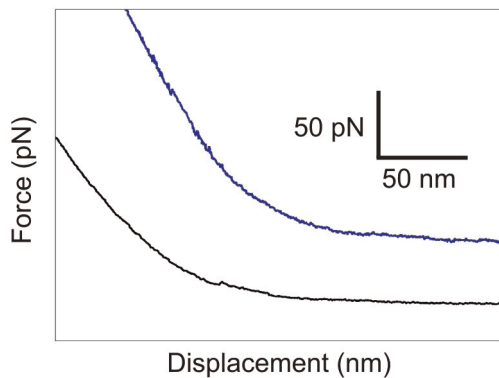
Fig. 2 Force–distance curves obtained during the retraction cycle of the indention. The absence of a pull-off force, or rupture force, indicates that there is no adhesion present between the sample and the indenter during experimentation

While in the current work only the elastic behaviour of RBCs is studied, RBCs have been found to exhibit viscoelastic behaviour under repetitive deformations [**49**]. The viscoelastic properties of normal RBCs have been studied via magnetic twisting cytometry. Results indicate that G', the storage modulus which represents the Young's modulus, is nearly constant for different frequencies, whereas G'', the loss modulus, increases with frequency [**50**]. This result suggests that the measurement of the effective Young's modulus presented in this work remains valid when repetitive loading is applied, at least for normal RBCs. Finally, it should be noted that AFM has been used to measure the viscoelastic behaviour of epithelial cells [**44**, **45**]. In principle, the used methods can be used to perform viscoelasticity measurements on normal and pathological RBCs.

3.2.1 Parabolic tip

When the shape of the AFM tip is approximated by a paraboloid with a radius of curvature R at the apex, the force $F_{\text{parabolic}}$ as a function of indentation u_z is described by the following equation [**40–42**]

$$F_{\text{parabolic}} = \frac{4}{3}\sqrt{RE'}\, u_z^{3/2} \tag{14}$$

where E' is the reduced Young's modulus of the tip–sample system defined as

$$\frac{1}{E'} = \frac{1 - v_{\text{sample}}^2}{E_{\text{tip}}} + \frac{1 - v_{\text{sample}}^2}{E_{\text{sample}}} \tag{15}$$

where E_{tip}, v_{tip}, and E_{sample}, v_{sample} are the Young's moduli and the Poisson's ratios for the materials of

the tip and the sample, respectively. If $E_{\text{sample}} \leq E_{\text{tip}}$ (in the case of Si_3N_4 tips, the Young's modulus is 150 GPa [**51**]), E' can be simplified to

$$E = \frac{E_{\text{sample}}}{1 - v_{\text{sample}}^2} \tag{16}$$

Poisson's ratio, v, is defined as the ratio of the transverse, or orthogonal, strain to the strain along the direction of elongation. It is useful for determining how much the material extends orthogonally to the direction in which the force is applied. The value of v is always between zero and 0.5 [**52**, **53**].

3.2.2 Pyramidal tip

When the shape of the AFM tip is a four-sided pyramidal indenter, the force F_{pyramid} as a function of indentation u_z is described by the following equation [**39**, **43–45**]

$$F_{\text{pyramid}} = \frac{3E\tan\theta}{4(1 - v^2)}\, u_z^2 \tag{17}$$

with an effective radius of contact $a = u_z\tan\theta / \sqrt{2}$ with θ defined as nominal angle of the pyramidal geometry [**43–45**].

4 METHODS

Experiments were carried out using an Asylum MFP 3D-BIO (Asylum Research, Santa Barbara, California) AFM equipped with a 'liquid cell' set-up.

4.1 RBC preparation

Whole blood was drawn from patients with SCD during clinical visits to the Lea Center for Hematologic Disorders at the University of Connecticut Health Center (UCHC) following the guidelines of the Human Subjects Protection Office at UCHC. Blood was drawn by venipuncture into 5 IU/ml heparin and centrifuged at 400 g for 15 min at 25 °C to isolate the RBCs. The yellowish supernatant containing plasma and the white fluffy coat on the pellet was discarded. All buffers were pre-warmed to 37 °C prior to use. RBCs were washed three times with phosphate-buffered saline (PBS) and finally re-suspended in PBS at a concentration of 5 per cent. Deoxygenated RBCs were obtained by bubbling N_2 through a suspension of RBCs in a sealed flask for 1 h. The state of deoxygenation of the erythrocytes was expected to be maintained for 1–1.5 h [**54**] and experiments were performed during this time.

4.2 Erythrocyte immobilization

Cells were immobilized on AFM grade mica (Novascan Technologies, Inc., Ames, Iowa) coated with poly-l-lysine (PLL) (Sigma-Aldrich, St. Louis, Missouri) to increase cell adherence. 150 μl of 1 mg/ml PLL solution was allowed to adsorb for 5 min to an unmodified mica surface, and excess solution was drained away. RBCs of 0.5 per cent concentration in PBS were allowed to adhere to each PLL-coated mica surface for 10 min in the incubator. Unattached cells were removed by gentle rinsing of the slide with PBS solution at 25 °C. For imaging, fixation was performed by a 1 min treatment of the cells with 0.5 per cent glutaraldehyde (Sigma-Aldrich, St. Louis, Missori) in PBS buffer. The sample was again rinsed several times with PBS and a volume of PBS was added for experiments. Glutaraldehyde was not employed for stiffness measurements.

4.3 Imaging

Erythrocytes were imaged in tapping mode with a scan rate of 0.2 Hz, and the minimal force necessary to obtain good image contrast was determined by gradually increasing the force applied to the sample from zero force (non-contact) to the necessary minimal force. Silicon nitride probes with a nominal spring constant of 0.01 N/m (Veeco Probes, Camarillo, California) were employed for imaging.

4.4 Measurements

Erythrocyte's stiffness measurements were carried out in contact mode using silicon nitride cantilevers with a nominal spring constant of 0.03 N/m (Veeco Probes, Camarillo, California). Exact values for the cantilever spring constants were obtained via a thermal-noise-based method implemented by the manufacturer and were used in all calculations. Probes had nominal tip radii R of 20 nm and nominal angle θ of 20°, as provided by the manufacturer. Tip height was 2.5 μm, as provided by the manufacturer. All measurements were performed in PBS at 25 °C. Local elastic properties of erythrocytes were quantitatively determined from the force–distance curves. The force curves were generated at a loading rate of 15 000 pN/s, and for both the oxygenated and deoxygenated states more than 500 measurements were collected.

4.5 Data processing

Data was imported into MATLAB (The MathWorks, Natick, Massachusetts) and the value of E was obtained by fitting the theoretical curves generated by equation (2) and equation (5) to the experimental data up to a minimum depth of 250 nm, which is approximately 10 per cent of the total thickness of the cell. The method is in agreement with the well-known fact that the effect of the substrate over which the cells are placed is negligible if the indentation depth is less than 10 per cent of the total thickness of the specimen [47].

5 RESULTS

5.1 Morphology of SCD erythrocytes via AFM imaging

Under both oxygenated and deoxygenated states, highly irregular morphologies were observed in the RBC samples. Normal RBCs are characterized by a biconcave shape which not only increases the surface area and facilitates O_2 and CO_2 diffusion into and out of the cell [55, 56] but also increases the compliance of the erythrocytes [57]. Polymerization of Hb fibres forces RBCs to assume a wide variety of irregular shapes [17]. Two representative examples are shown in Fig. 3. Repeated cycles of oxygenation and deoxygenation lead to irreversible sickling, a phenomenon that it is thought to have occurred to the erythrocyte in Fig. 3(a), imaged under oxygenated conditions. This cell is characterized by protrusions likely resulting from polymerized Hb fibres and also an enlarged morphology. Upon deoxygenation, as in Fig. 3(b), HbS fibres are expected to polymerize and aggregate, thus forming the highly elongated and irregular structure shown. In addition, this cell also contains bumps and surface irregularities which are possibly associated with protruding polymerized HbS fibres and changes in the RBC membrane cortex.

5.2 Determination of the indentation depth

The quantitative determination of the elastic properties of a particular material can be obtained from the relationship between the applied force F and the indentation depth δ using equation (14) and equation (17). When force is measured on a hard substrate, the cantilever deflection is proportional to the relative sample position resulting in a linear slope for the portion of the curve where the tip and the sample are in contact. When soft samples such as erythrocytes are investigated, the recorded cantilever deflection as a function of the relative sample position is not linear owing to the deformable structure of the RBC. Prior to taking force measurements on the RBC surface, the force is measured on the PLL-coated mica substrate. This curve is used for calibration since no permanent sample deformation
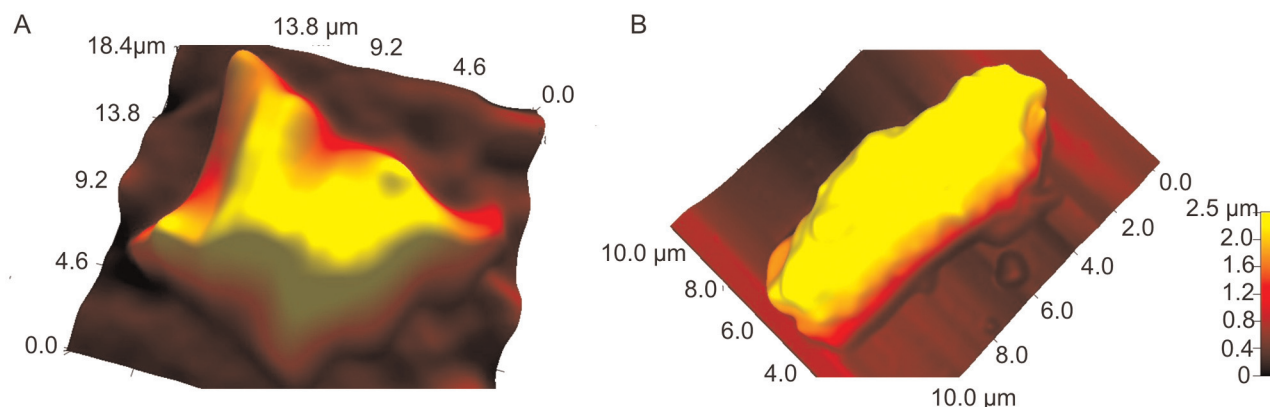
Fig. 3 Three-dimensional topographical images of (a) a SCD erythrocyte in an oxygenated environment and (b) a SCD erythrocyte in a fully deoxygenated state measured via AFM. Both RBCs have a highly irregular morphology as compared to the characteristic biconcave shape of a normal erythrocytes. It is evident that polymerized Hb results in highly irregular RBC morphologies characterized by protrusions, elongation, bumps, and enlargement associated with aggregation of HbS fibres

is observed. The indentation produced by the AFM tip was determined by subtracting the calibration curve from the curve recorded for the erythrocyte using the Igor Pro 6.04 (Wavemetrics, Portland, Oregon) software program.

5.3 Force–displacement curve analysis

The Matlab output of both the pyramidal indenter model obtained from equation (17) and the parabolic indenter model obtained from equation (14) fit to the force versus indentation curve obtained via experimentation is shown in Fig. 4. The model of the pyramid indenter appears to provide a better fit, as shown by the representative curves shown in Fig. 4. At small Young's modulus values ($E < 3$ kPa), as in Figs 4(a) and (b), both the pyramid model and the parabolic model appear to fit the experimental force–displacement curves to a minimum depth of 250 nm, which is approximately 10 per cent of the thickness of the cell [41].

However, as indentation continues, the pyramid model continues to follow the trend of the experimental force–displacement curves whereas the paraboloid model greatly diverges. As the stiffness of the erythrocyte's increased, the pyramid model continued to provide a more accurate fit to the experimental data as shown in Figs 4(c) and (d). Although the paraboloid model appears to fit the data up to 50 nm indentations, the pyramid model continues to fit the data up to approximately 250 nm, representative of 10 per cent of the total thickness of the cell. Based on the presented theoretical model it was decided to continue the cell stiffness analysis via the model for the four-sided pyramidal indenter.

5.4 Cell stiffness determination

A representative curve showing experimental data for erythrocytes from patients with SCD is shown in Fig. 5(a). This data was fitted to the theoretical pyramid model and theoretical pyramid model curves representative of normal and SCT erythrocytes are also shown for comparison. The average values of the Young's modulus for oxygenated and deoxygenated SCD erythrocytes were obtained by fitting a Gaussian distribution to the generated histograms of the measured Young's modulus values (Fig. 5(b)). It appears that both oxygenated and deoxygenated SCD RBCs maintain a bimodal distribution with peaks at $E_1 = 1.0 \pm 1.1$ kPa, and $E_2 = 3.0 \pm 2.7$ kPa. A similar value has been reported that was obtained using optical tweezers [58]. By overlaying the histogram of the distribution of oxygenated SCD erythrocyte elasticity values on top of the normal and SCT distribution, it is evident that each peak in the focused SCD erythrocyte distribution corresponds to the same Young's modulus value as the SCT and normal RBCs, 3.0 and 1.0 kPa, respectively [33]. As seen in Fig. 6, oxygenated RBCs have an additional peak at approximately 15 kPa, whereas deoxygenated RBCs have an additional peak at approximately 40 kPa.

6 DISCUSSION

The Young's modulus is the basic material coefficient of elasticity. It can range from ~100 GPa for high-strength materials (steel, titanium) [59, 60] to 100s MPa for typical polymers (polystyrene), and 1 MPa for soft gel-like materials (gelatin in its
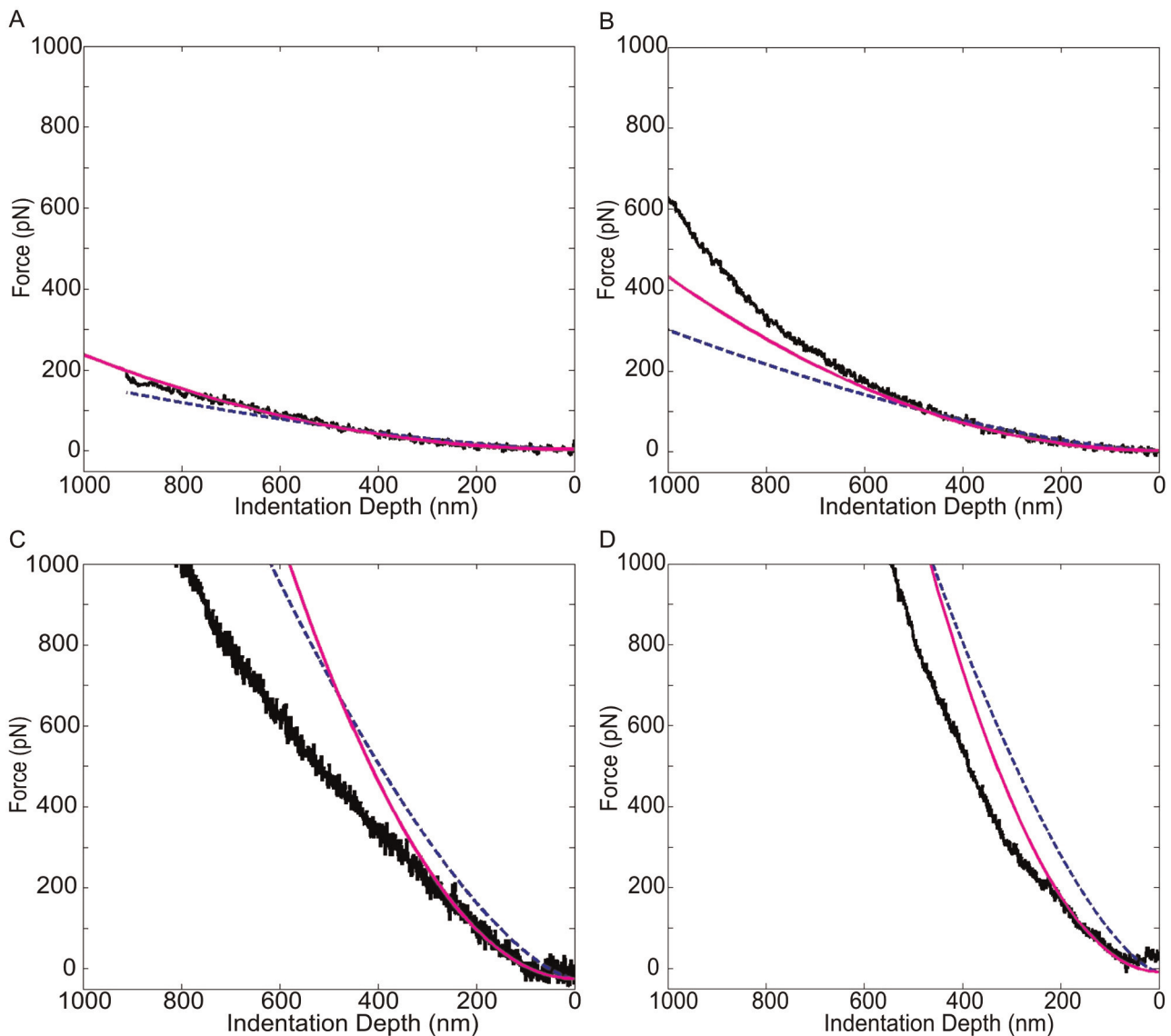
Fig. 4 Theoretical models for a pyramid indenter and a parabolic indenter fitted to the experimental data for clinical SCD erythrocytes obtained via AFM. In these curves, the Young's modulus values are (a) 0.65 kPa, (b) 1.20 kPa, (c) 8.50 kPa, and (d) 13.0 kPa. These curves are representative of the force curves obtained for all SCD clinical samples of varying stiffness values. From the given data at a broad range of Young's modulus values, it appears that the pyramid indenter model provides a better fit. Legend in (a) applies for all

gel-phase) [60]. Typical values for cells range from 1 to 100 kPa [7, 8, 61–67]. In the present study, it has been shown that sickle erythrocytes possess Young's modulus values between 1 and 60 kPa depending on their degree of oxygenation and the percentage of HbS present in the erythrocytes. Both oxygenated and deoxygenated samples of RBCs from patients with SCD maintain a bimodal distribution with peaks representative of normal RBCs ($E_1 = 1.0 \pm 1.1$ kPa) and SCT RBCs ($E_2 = 3.0 \pm 2.7$ kPa) [33]. Evidence of an additional peak is also present for both oxygenated and deoxygenated samples at

$E = 15$ kPa and $E = 40$ kPa, respectively. The large variation and presence of multiple peaks within the distribution can be possibly attributed to patient treatment with hydroxyurea.

Significantly higher Young's modulus values resulting in peaks at $E = 15$ kPa for oxygenated cells and $E = 40$ kPa for deoxygenated cells are a result of the presence of polymerized HbS in the RBC samples from SCD patients. At high concentrations, deoxy sickle hemoglobin results in the formation of a seven-stranded polymer structure which increases RBC rigidity [68]. Polymerization of deoxygenated
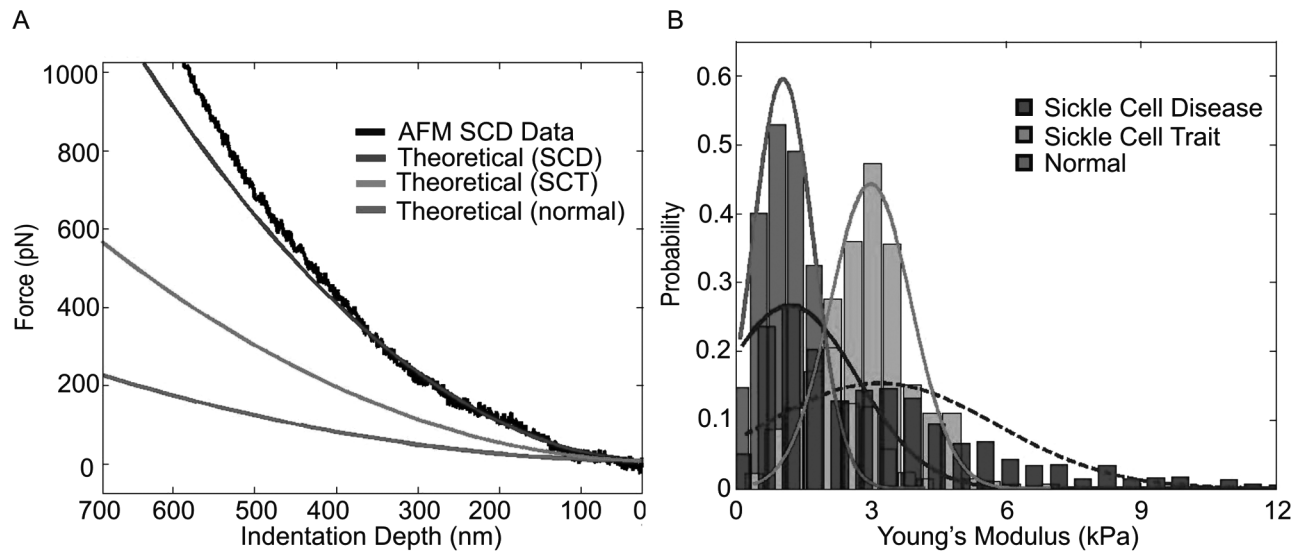
A

B

Fig. 5 Experimental data for Young's modulus. (a) The data shows the theoretical pyramid model (equation (4)) fitted to the experimental data for normal, SCT, and SCD erythrocytes. In these curves, the Young's modulus values for the normal, SCT, and both oxygenated and deoxygenated SCD RBCs are 1.30, 3.30, and 7.0 kPa, respectively. Curves shown are representative of the 500–600 force curves obtained for each normal and SCT RBCs, and 1000+ curves for SCD clinical samples. (b) Histograms of the Young's modulus values determined for RBCs from normal, SCT, and both oxygenated and deoxygenated SCD erythrocytes. Values for normal RBCs are $E_{normal} = 1.10 \pm 0.40$ kPa and SCT RBCs are $E_{SCT} = 3.05 \pm 1.09$ kPa. SCD clinical samples reveal a bimodal distribution with $E_1 = 1.0 \pm 1.1$ kPa, and $E_2 = 3.0 \pm 2.7$ kPa, as well as higher ($E > 7.0$ kPa) values
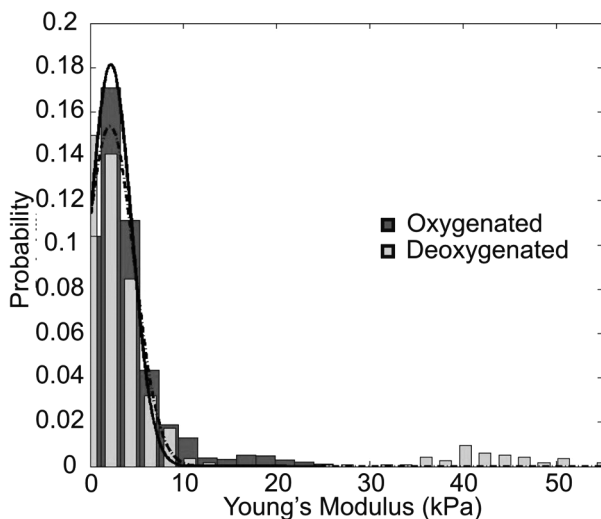

Fig. 6 Histograms of the Young's modulus determined for SCD RBCs maintained in oxygenated and deoxygenated environments. The Young's modulus values obtained from fitting the theoretical pyramid indenter model to the experimental data were fitted with the Gaussian distribution. The full distribution shows evidence of an additional peak appearing around 15 kPa for the oxygenated RBCs and 40 kPa for the deoxygenated RBCs

HbS is dependent on intraerythrocytic HbS concentration, degree of cell oxygenation, pH, and the intracellular concentration of HbF. Polymerized HbS fibres form non-covalent cross-links and create a gel that results in increased rigidity of RBCs [**16**, **18–21**]. In addition, spectrin, which is the main protein responsible for the mechanical strength of the erythrocyte, has been found to bind to hemoglobin via the band 3 protein that binds almost exclusively to hemoglobin fibres [**32**, **69**]. Thus, in the deoxygenated state, interaction between the HbS fibres that are connected to the membrane and the HbS fibres in the cytoplasm could also contribute to the measured increase in stiffness [**70**]. The data obtained in this study shows evidence of a minimal doubling of the Young's modulus upon full deoxygenation of SCD erythrocytes. This can present major problems in SCD patients because rigid sickle RBC can cause microcirculatory obstruction, resulting in vaso-occlusive crisis.

The small Young's modulus values found in the present study for both oxygenated and deoxygenated SCD erythrocytes are likely due to hydroxyurea treatment, a variable in the obtained clinical samples. Hydroxyurea is the only approved medication

for the treatment of SCD in adults; there are no approved drugs for children [71, 72]. Hydroxyurea stimulates the production of fetal hemoglobin (HbF) in patients with SCD, which inhibits sickling [73] by preventing effective contact between adjacent HbS molecules and also by forming mixed hybrids with HbS that have greater solubility than HbS polymers [72]. Increases in HbF contribute to an increase in total Hb and a decrease in hemolysis with the release of free hemoglobin [71]. It has been proposed that hydroxyurea increases HbF indirectly by killing rapidly dividing late erythroid cells, causing recruitment of more primitive erythroid precursors which in turn produce high levels of HbF, or by acting directly on the primitive precursors thereby stimulating HbF production, the exact mechanism by which hydroxyurea induces HbF is unclear [72].

7 CONCLUSIONS

In summary, the present study suggests a significant impact of deoxy sickle hemoglobin in significantly increasing the rigidity of SCD erythrocytes, thus resulting in vaso-occlusive crisis. The presented data leads to the conclusion that Young's moduli and standard deviations were $E_1 = 1.0 \pm 1.1$ kPa and $E_2 = 3.0 \pm 2.7$ kPa for both oxygenated and deoxygenated SCD erythrocytes. Deoxygenated SCD erythrocytes also possessed an additional peak at $E = 40$ kPa, whereas oxygenated SCD erythrocytes possessed an additional peak at the significantly lower value of $E = 15$ kPa. However, in contrast to normal RBCs and SCT RBCs, SCD erythrocytes substantially deviate from the characteristic biconcave shape and possess highly irregular morphologies characterized by protrusions, elongation, bumps, and enlargement associated with aggregation of HbS fibres.

REFERENCES

1   **Janmey, P. A.** The cytoskeleton and cell signaling: component localization and mechanical coupling. *Physiol. Rev.*, 1998, **78**(3), 763–781.
2   **Huang, S.** and **Ingber, D. E.** The structural and mechanical complexity of cell-growth control. *Nature Cell Biol.*, 1999, **1**(5), E131–E138.
3   **Binnig, G., Quate, C. F.,** and **Gerber, C.** Atomic force microscope. *Phys. Rev. Lett.*, 1986, **56**, 930–933.
4   **Suresh, S.** Nanomedicine - elastic clues in cancer detection. *Nature Nanotechnol.*, 2007, **2**(12), 748–749.

5   **Radmacher, M.** Measuring the elastic properties of biological samples with the AFM. *IEEE Engng Med. Biol. Mag.*, 1997, **16**(2), 47–57.
6   **Rotsch, C., Braet, F., Wisse, E.,** and **Radmacher, M.** *et al.* AFM imaging and elasticity measurements on living rat liver macrophages. *Cell Biol. Int.*, 1997, **21**(11), 685–696.
7   **Radmacher, M., Fritz, M., Kacher, C. M., Cleveland, J. P.,** and **Hansma, P. K.** Measuring the viscoelastic properties of human platelets with the atomic force microscope. *Biophys. J.*, 1996, **70**(1), 556–567.
8   **Cross, S. E., Jin, Y. S., Rao, J.,** and **Gimzewski, J. K.** Nanomechanical analysis of cells from cancer patients. *Nature Nanotechnol.*, 2007, **2**(12), 780–783.
9   **Iyer, S., Gaikwad, R. M., Subba-Rao, V., Woodworth, C. D.,** and **Sokolov, I.** Atomic force microscopy detects differences in the surface brush of normal and cancerous cells. *Nature Nanotechnol.*, 2009, **4**(6), 389–393.
10 **Li, Q. S., Lee, G. Y. H., Ong, C. N.,** and **Lim, C. T.** AFM indentation study of breast cancer cells. *Biochem. Biophys. Res. Commun.*, 2008, **374**(4), 609–613. DOI: 10.1016/j.bbrc.2008.07.078.
11 **Buehler, M. J.** and **Yung, Y. C.** Deformation and failure of protein materials in physiologically extreme conditions and disease. *Nature Mater.*, 2009, **8**(3), 175–188.
12 **Steinberg, M. H.** and **Brugnara, C.** Pathophysiological-based approaches to treatment of sickle cell disease. *Ann. Rev. Med.*, 2003, **54**(1), 89–112.
13 **Alberts, B., Johnson, A., Lewis, J., Ralf, M., Roberts, K.,** and **Walter, P.** *Molecular biology of the cell*, 2002 (Garland, New York).
14 **Ferrone, F. A.** Polymerization and sickle cell disease: a molecular view. *Microcirculation*, 2004, **11**(2), 115–128.
15 **Noguchi, C. T.** and **Schechter, A. N.** Sickle hemoglobin polymerization in solution and in cells. *Ann. Rev. Biophys. Biophys. Chem.*, 1985, **14**, 239–263.
16 **Turner, M. S., Wang, J. C., Jones, C. W., Ferrone, F. A., Josephs, R.,** and **Briehl, R. W.** Fluctuations in self-assembled sickle hemoglobin fibers. *Langmuir*, 2002, **18**(19), 7182–7187.
17 **Christoph, G. W., Hofrichter, J.,** and **Eaton, W. A.** Understanding the shape of sickled red cells. *Biophys. J.*, 2005, **88**(2), 1371–1376.
18 **Wang, J. C., Turner, M. S., Agarwal, G., Kwong, S., Josephs, R., Ferrone, F. A.,** and **Briehl, R. W.** Micromechanics of isolated sickle cell hemoglobin fibers: bending moduli and persistence lengths. *J. Molec. Biol.*, 2002, **315**(4), 601–612.
19 **Jones, C. W., Wang, J. C., Ferrone, F. A., Briehl, R. W.,** and **Turner, M. S.** Interactions between sickle hemoglobin fibers. *Faraday Discuss.*, 2003, **123**, 221–236.
20 **Aprelev, A., Rotter, M. A., Etzion, Z., Bookchin, R. M., Briehl, R. W.,** and **Ferrone, F. A.** The effects of erythrocyte membranes on the nucleation of sickle hemoglobin. *Biophys. J.*, 2005, **88**(4), 2815–2822.

21 **Wang, J. C., Kwong, S., Ferrone, F. A., Turner, M. S.,** and **Briehl, R. W.** Fiber depolymerization: fracture, fragments, vanishing times, and stochastics in sickle hemoglobin. *Biophys. J.*, 2009, **96**(2), 655–670.

22 **Connes, P., Reid, H., Hardy-Dessources, M. D., Morrison, E.,** and **Hue, O.** Physiological responses of sickle cell trait carriers during exercise. *Sports Med.*, 2008, **38**(11), 931–946.

23 **Embury, S. H.** The clinical pathophysiology of sickle-cell disease. *Ann. Rev. Med.*, 1986, **37**, 361–376.

24 **Kaul, D. K., Fabry, M. E.,** and **Nagel, R. L.** The pathophysiology of vascular obstruction in the sickle syndromes. *Blood Rev.*, 1996, **10**(1), 29–44.

25 **Ballas, S. K.** and **Mohandas, N.** Pathophysiology of vaso-occlusion. *Hematol.-Oncol. Clinics N. Am.*, 1996, **10**(6), 1221–1239.

26 **Neel, J. V., Wells, I. C.,** and **Itano, H. A.** Familial differences in the proportion of abnormal hemoglobin present in the sickle cell trait. *J. Clin. Invest.*, 1951, **30**(10), 1120–1124.

27 **Wells, I. C.** and **Itano, H. A.** Ratio of sickle-cell anemia hemoglobin to normal hemoglobin in sicklemics. *J. Biol. Chem.*, 1951, **188**(1), 65–74.

28 **Mohandas, N.** and **Evans, E.** Mechanical-properties of the red-cell membrane in relation to molecular-structure and genetic-defects. *Ann. Rev. Biophys. Biomed.*, 1994, **23**, 787–818.

29 **Statius Van Eps, L. W.** Sickle cell disease. In *Atlas of diseases of the kidney* (Ed. Schrier, R. W.), vol. 4, Current Medicine, Inc., Philadelphia, 1999.

30 **Fortier, N., Snyder, L. M., Garver, F., Kiefer, C., McKenney, J.,** and **Mohandas, N.** The relationship between in vivo generated hemoglobin skeletal protein complex and increased red-cell membrane rigidity. *Blood*, 1988, **71**(5), 1427–1431.

31 **Snyder, L. M., Leb, L., Piotrowski, J., Sauberman, N., Liu, S. C.,** and **Fortier, N. L.** Irreversible spectrin hemoglobin crosslinking in vivo - a marker for red-cell senescence. *Br. J. Haematol.*, 1983, **53**(3), 379–384.

32 **Walder, J. A., Chatterjee, R., Steck, T. L., Low, P. S., Musso, G. F., Kaiser, E. T., Rogers, P. H.,** and **Arnone, A.** The interaction of hemoglobin with the cytoplasmic domain of band-3 of the human-erythrocyte membrane. *J. Biol. Chem.*, 1984, **259**(16), 238–246.

33 **Maciaszek, J. L.** and **Lykotrafitis, G.** Sickle cell trait erythrocytes are significantly stiffer than normal. *J. Biomech.*, 2011, **44**(4), 657–661.

34 **Timoshenko, S. P.** and **Goodier, J. N.** *Theory of elasticity*, third edition, 1970 (McGraw-Hill, New York).

35 **Hertz, H.** On the contact of elastic solids. *J. Reine Ang. Math.*, 1881, **92**, 156–171.

36 **Sneddon, I.** The relation between load and penetration in axisymmetric Boussinesq problem for a punch of arbitrary profile. *Int. J. Engng Sci.*, 1965, **3**, 47–57.

37 **Barber, J. R.** and **Billings, D. A.** An approximate solution for the contact area elastic compliance of a smooth punch of arbitrary shape. *Int. J. Mech. Sci.*, 1990, **32**(12), 991–997.

38 **Barber, J. R.** Determining the contact area in elastic-indentation problems. *J. Strain Anal.*, 1974, **9**(4), 230–232.

39 **Giannakopoulos, A. E.** Elastic and viscoelastic indentation of flat surfaces by pyramid indentors. *J. Mech. Phys. Solids*, 2006, **54**(7), 1305–1332.

40 **Dulinska, I., Targosz, M., Strojny, W., Lekka, M., Czuba, P., Balwierz, W.,** and **Szymonski, M.** Stiffness of normal and pathological erythrocytes studied by means of atomic force microscopy. *J. Biochem. Biophys. Methods*, 2006, **66**(1–3), 1–11.

41 **Hategan, A., Law, R., Kahn, S.,** and **Discher, D. E.** Adhesively-tensed cell membranes: lysis kinetics and atomic force microscopy probing. *Biophys. J.*, 2003, **85**(4), 2746–2759.

42 **Kuznetsova, T. G., Starodubtseva, M. N., Yegorenkov, N. I., Chizhik, S. A.,** and **Zhdanov, R. I.** Atomic force microscopy probing of cell elasticity. *Micron*, 2007, **38**, 824–833.

43 **Bilodeau, G. G.** Regular pyramid punch problem. *J. Appl. Mech.*, 1992, **59**(3), 519–523.

44 **Rico, F., Roca-Cusachs, P., Gavara, N., Farre, F., Rotger, M.,** and **Navajas, D.** Probing mechanical properties of living cells by atomic force microscopy with blunted pyramidal cantilever tips. *Phys. Rev. E, Stat. Nonlinear Sost Matter Phys.*, 2005, **72**(2), 1–10.

45 **Alcaraz, J., Buscemi, L., Grabulosa, M., Trepat, X., Fabry, B., Farre, R.,** and **Navajas, D.** Microrheology of human lung epithelial cells measured by atomic force microscopy. *Biophys. J.*, 2003, **84**(3), 2071–2079.

46 **Mahaffy, R. E., Shih, C. K., Mackintosh, F. C.,** and **Kas, J.** Scanning probe-based frequency-dependent microrheology of polymer gels and biological cells. *Phys. Rev. Lett.*, 2000, **85**(4), 880–883.

47 **Dimitriadis, E. K., Horkay, F., Maresca, J., Kachar, B.,** and **Chadwick, R. S.** Determination of elastic moduli of thin layers of soft material using the atomic force microscope. *Biophys. J.*, 2002, **82**(5), 2798–2810.

48 **Johnson, K. L., Kendall, K.,** and **Roberts, A. D.** Surface energy and the contact of elastic solids. *Proc. Roy. Soc. Lond. A, Math. Phys. Sci.*, 1971, **324**(1558), 301–313.

49 **Puig-de-Morales-Marinkovic, M., Turner, K. T., Butler, J. P., Fredberg, J. J.,** and **Suresh, S.** Viscoelasticity of the human red blood cell. *Am. J. Physiol.-Cell Physiol.*, 2007, **293**(2), C597–C605.

50 **Zhu, C., Bao, G.,** and **Wang, N.** Cell mechanics: mechanical response, cell adhesion, and molecular deformation. *Ann. Rev. Biomed. Engng*, 2000, **2**, 189–226.

51 **Vinckier, A.** and **Semenza, G.** Measuring elasticity of biological materials by atomic force microscopy. *FEBS Lett.*, 1998, **430**(1–2), 12–16.

52 **Heuberger, M., Dietler, G.,** and **Schlapbach, L.** Mapping the local Young's modulus by analysis of the elastic deformations occurring in atomic-force microscopy. *Nanotechnology*, 1995, **6**(1), 12–23.

53 **Vanlandingham, M. R., Mcknight, S. H., Palmese, G. R., Elings, J. R., Huang, X., Bogetti, T. A., Eduljee, R. F.,** and **Gillespie, J. W.** Nanoscale indentation of polymer systems using the atomic force microscope. *J. Adhes.*, 1997, **64**(1-4), 31–59.

54 **Tuvia, S., Levin, S.,** and **Korenstein, R.** Oxygenation-deoxygenation cycle of erythrocytes modulates submicron cell-membrane fluctuations. *Biophys. J.*, 1992, **63**(2), 599–602.

55 **Mohandas, N.** and **Gallagher, P. G.** Red cell membrane: past, present, and future. *Blood*, 2008, **112**(10), 3939–3948.

56 **Alberts, B., Bray, D., Lewis, J., Raff, M., Roberts, K.,** and **Walter, P.** Molecular biology of the cell, 1983 (Garland Science, London).

57 **Li, J., Dao, M., Lim, C. T.,** and **Suresh, S.** Spectrin-level modeling of the cytoskeleton and optical tweezers stretching of the erythrocyte. *Biophys. J.*, 2005, **88**(5), 3707–3719.

58 **Dao, M., Lim, C. T.,** and **Suresh, S.** Mechanics of the human red blood cell deformed by optical tweezers. *J. Mech. Phys. Solids*, 2003, **51**(11-12), 2259–2280.

59 **Gray, D. E.** *American Institute of Physics handbook*, 1972 (McGraw-Hill, New York).

60 **Fung, Y. C.** *Biomechanics: mechanical properties of living tissues*, 1981 (Springer, New York).

61 **Cai, X. F., Xing, X. B., Cai, J. Y., Chen, Q., Wu, S.,** and **Huang, F.** Connection between biomechanics and cytoskeleton structure of lymphocyte and jurkat cells: an AFM study. *Micron*, 2010, **41**(3), 257–262.

62 **Cai, X. F., Yang, X. X., Cai, J. Y., Wu, S.,** and **Chen, Q.** Atomic force microscope-related study membrane-associated cytotoxicity in human pterygium fibroblasts induced by mitomycin c. *J. Phys Chem B*, 2010, **114**(11), 3833–3839.

63 **Schafer, A.** and **Radmacher, M.** Influence of myosin ii activity on stiffness of fibroblast cells. *Acta Biomater.*, 2005, **1**(3), 273–280.

64 **Yim, E. K. F., Darling, E. M., Kulangara, K., Guilak, F.,** and **Leong, K. W.** Nanotopography-induced changes in focal adhesions, cytoskeletal organization, and mechanical properties of human mesenchymal stem cells. *Biomaterials*, 2010, **31**(6), 1299–1306.

65 **Domke, J., Dannohl, S., Parak, W. J., Muller, O., Aicher, W. K.,** and **Radmacher, M.** Substrate dependent differences in morphology and elasticity of living osteoblasts investigated by atomic force microscopy. *Colloids Surf. B, Biointerfaces*, 2000, **19**(4), 367–379.

66 **Simon, A., Cohen-Bouhacina, T., Porte, M. C., Aime, J. P., Amedee, J., Bareille, R.,** and **Baguey, C.** Characterization of dynamic cellular adhesion of osteoblasts using atomic force microscopy. *Cytometry. Part A: J. Inter. Soc. Analytical Cytology*, 2003, **54**(1), 36–47.

67 **Takai, E., Costa, K. D., Shaheen, A., Hung, C. T.,** and **Guo, X. E.** Osteoblast elastic modulus measured by atomic force microscopy is substrate dependent. *Ann. Biomed. Engng*, 2005, **33**(7), 963–971.

68 **Turner, M. S., Briehl, R. W., Wang, J. C., Ferrone, F. A.,** and **Josephs, R.** Anisotropy in sickle hemoglobin fibers from variations in bending and twist. *J. Molec. Biol.*, 2006, **357**(5), 1422–1427.

69 **von Ruckmann, B., Jons, T., Dolle, F., Drenckhahn, D.,** and **Schubert, D.** Cytoskeleton-membrane connections in the human erythrocyte membrane: band 4.1 binds to tetrameric band 3 protein. *Biochim. Biophys. Acta, Biomembranes*, 1997, **1325**(2), 226–234.

70 **Brugnara, C.** Red cell membrane in sickle cell disease. In *Disorders of hemoglobin: genetics, pathophysiology, and clinical management* (Eds M. H. Steinberg, B. G. Forget, D. R. Higgs, and R. L. Nagel), 2001, pp. 550–576 (Cambridge University Press, New York).

71 **Strouse, J. J., Lanzkron, S., Beach, M. C., Haywood, C., Park, H., Witkop, C., Wilson, R. F., Bass, E. B.,** and **Segal, J. B.** Hydroxyurea for sickle cell disease: a systematic review for efficacy and toxicity in children. *Pediatrics*, 2008, **122**(6), 1332–1342.

72 **Halsey, C.** and **Roberts, I. A. G.** The role of hydroxyurea in sickle cell disease. *Br. J. Haematol.*, 2003, **120**(2), 177–186.

73 **Charache, S., Dover, G. J.,** and **Moore, R. D.** *et al.* Hydroxyurea – effects on hemoglobin-f production in patients with sickle-cell-anemia. *Blood*, 1992, **79**(10), 2555–2565.

APPENDIX

Notation

a	radius of contact of tip with sample
A	contact region of indentation
$\bar{A}$	separation region of indentation
d	deflection of cantilever on the indented half-space
E	Young's modulus
E'	reduced Young's modulus
E_1	Young's modulus of first bimodal peak of oxy- and deoxy- samples
E_2	Young's modulus of second bimodal peak of oxy- and deoxy- samples
E_{normal}	Young's modulus of normal erythrocytes
E_{sample}	Young's modulus of the sample
E_{SCT}	Young's modulus of SCT erythrocytes
E_{tip}	Young's modulus of the tip
f	profile of the punch
F	force
$F_{parabolic}$	force approximated by parabolic tip
$F_{pyramid}$	force approximated by pyramidal tip
g	gap between the punch and the half-space

G'	storage modulus	ν	Poisson's ratio
G''	loss modulus	ν_{sample}	Poisson's ratio of the sample
p	contact pressure	ν_{tip}	Poisson's ratio of the tip
P_z	total contact force	δ	deflection of the cantilever on the rigid substrate
r_{s}	radius of spherical tip		
R	radius of curvature of tip	Y	nominal angle of tip
u_z	normal deformation of the indented elastic half-space surface	σ	tangential traction on half-space